A.S.M.E.
Human Powered Vehicle
Design Report

A.S.M.E. East Coast and Midwest Competition

Emily Green
Jess Henning
Marc Hopkins
Ben Kuipers
Michael Lestingi
George Lyons

LAFAYETTE
A NATIONAL REPUTATION FOR ACADEMIC EXCELLENCE

Table of Contents

Abstract

The American Society of Mechanical Engineers' (ASME) Human Powered Vehicle (HPV) competition challenges teams to design and fabricate a vehicle, following ASME guidelines, to safely compete in the HPV endurance and sprint races.

In this, the inaugural year of Lafayette's participation in the HPV competition, the student team engineered unique, cost efficient solutions to the complex task of harnessing mechanical advantage to propel a human quickly and safely under her/his own power. The process has been documented, equitable, and timely. The team's efforts focused on design, analysis, testing, and safety. Additionally, the fabrication process was student-centered; all items not purchased were manufactured by the team members under the supervision of Lafayette College technicians.

The design process was cooperative and productive. Using collaborative brainstorming sessions, literature review, and modern design software, the team was able to efficiently explore vehicle options and select appropriate engineering solutions. Autodesk Inventor 7 ® enabled the team to parametrically model design concepts at various stages. Capitalizing on the ease and versatility of the software, the HPV design team was able to rapidly consider and implement design modifications.

Simple first-order analyses helped to add focus to the initial design process. Ultimately, the team utilized the Finite Element Method to refine preliminary designs. ANSYS 7.1 ®, a full package Finite Element Analysis program, was employed to this end. Additional analysis methodologies included graphical and empirical techniques. The analyses conducted yielded significant results, which were used to make meaningful changes to the HPV design.

While empirical results and engineering analyses provide a sound basis for design, prototype testing was crucial to the development and verification of the final product. Testing results were used to analyze and optimize the HPV. Testing helped to simulate and prepare for actual competition conditions and thusly, aided in confirming the team's analyses. With this confirmation came confidence in the performance and safety of the vehicle. Attention to safety and hazard reduction was paramount in the planning and production of a competitive HPV.

I. Innovation and Design

As this is the first year of Lafayette's participation in the HPV competition, the college's team was faced with the challenge of innovating an original design without the benefit of past experience. The HPV team members have worked cooperatively, using consensus building meetings to facilitate shared leadership. Traditional hierarchical approaches to team leadership were not only unnecessary, but by setting them aside, the team was able to avoid the perils of groupthink, producing a better final product.

To facilitate the design process, the team parametrically modeled the HPV using AutoDesk Inventor 7®. This modeling technique enabled the team to smoothly proceed along the iterative process of engineering design. What emerged is a two-wheeled, semi-recumbent vehicle with a partial solid fairing and ability to adjust to riders of different height.

A. Design Methodology

1. Objective

Care was taken to clearly define the goals and constraints of the project before the team engineered solutions to meet these goals. Solution requirements were related to performance, safety and documentation. Goals and constraints were mapped to show interrelatedness; this process focused and streamlined the development of engineering solutions. *Figure I.1* shows an example of a goal/constraint dependency map for the goal of "fast." Arrows (➢) indicate characteristics that affect the goal and square bullets (■) are design considerations that govern those characteristics. Similar goal/constraint dependency maps were constructed for the goals: safe, reliable and economic.

FAST

➢ Aerodynamic Drag (low)
- Fairing (shape)
- Dimensions
- Seating position

➢ Seat Adjustment for Max Power (rapid)
- Wheel clearances
- Frame geometry

➢ Entrance/exit (rapid)
- Free feet
- Adjustable seat
- Fairing (shape)

➢ Internal friction (low)
- Lubrication
- Pulleys
- Drive train (width)
- Bottom bracket bearings

➢ Wheel frictions (minimize slip)
- Back/front tire
- Weight distribution (normal force)
- Wheel surface

➢ Internal power loss
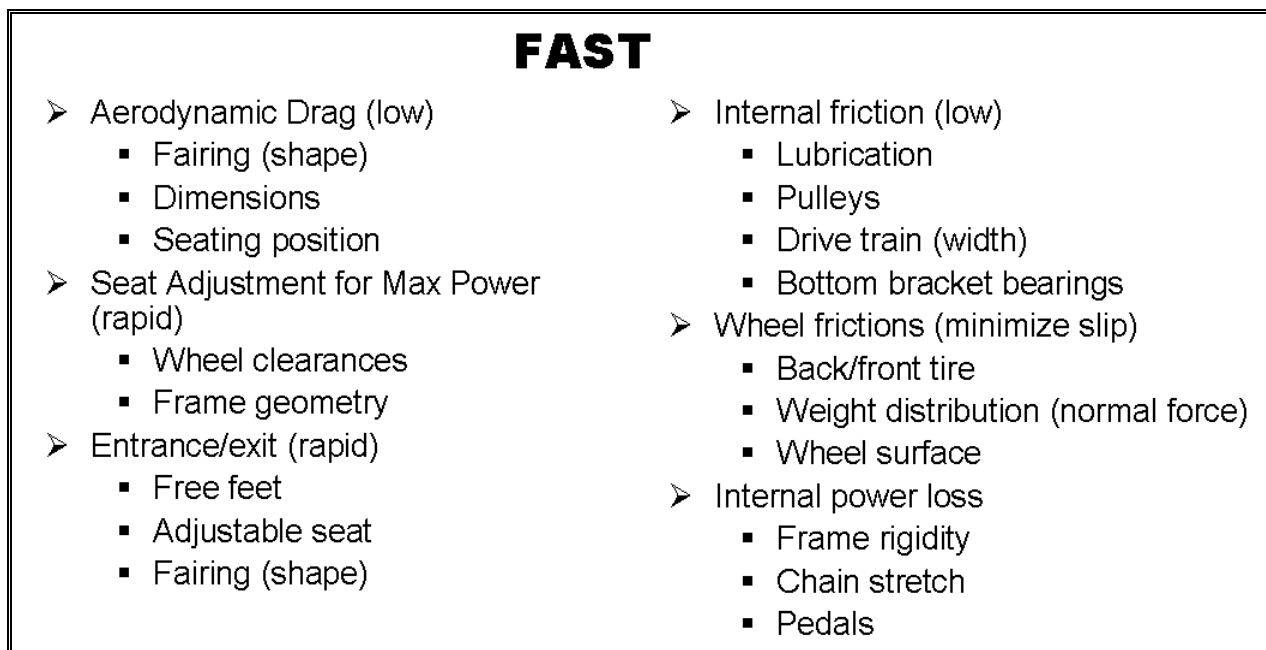- Frame rigidity
- Chain stretch
- Pedals

Figure I.1 Goal/constraint map for goal "fast."

2. Design Criteria / Outcome Targets

To facilitate the design process numerical target outcomes were established. These targeted minima and maxima are selected from the HPV rules and regulations or are calculated from empirical results of past HPV competitions. *Table I.1* summarizes these outcome targets.

Table I. 1 Target Minima and Maxima.

VARIABLE	DESCRIPTION	VALUE	MIN/MAX	JUSTIFICATION
V_g	Peak Ground Velocity	17 m/s	Min	Empirical
R_T	Turning Radius	25 feet	Max	ASME rules
S_B	Breaking Distance	20 ft at 15 mph	Max	ASME rules
C_D	Drag Coefficient	0.18	Max	See *Addendum C*

In establishing a goal for the peak achievable HPV ground velocity, the team considered the published results of the past three ASME HPV competitions as well as the maximum speed achieved on an upright bicycle found during the biomechanical testing of Lafayette's team (See *Section III.A, Testing after Fabrication*). The abbreviated results of the HPV sprint competitions are presented in *Table I.2*. As this table illustrates, the average speed of a winning vehicle is 17 m/s. The average speed of all competing vehicles is reported as nominally 12 m/s. Taking into account that our fastest rider is capable of reaching a speed of 13 m/s on level ground with an unfaired upright bicycle, the team reasoned that a goal of 17 m/s should be established for the peak ground velocity, i.e., the sprint velocity.

Table I. 2 Abbreviated Results of ASME HPV Sprint Competitions 2001 – 2003.

Average Velocity for All Competitors (m/s)	Average Winning Velocity (m/s)
11.7	17.0

The goals for turning radius and braking distance are requirements set forth by ASME. Meeting these requirements will allow the team to safely and quickly navigate the endurance and sprint courses; thus the team adopted them directly as target values.

Recognizing that approximately 85 percent of rider power is utilized to overcome drag (Martin 2003), the team identified the vehicle drag coefficient as a significant variable. Experimental data regarding each group member's respective power output was collected using a stationary recumbent exercise bicycle. Calculations were performed to determine the power necessary for each team member to reach the target sprint velocity. These calculations are presented in *Addendum C, Aerodynamic Calculations*. As *Figure I.2* illustrates, Lafayette's fastest rider requires a drag coefficient less than or equal to 0.18 to reach the target maximum velocity.
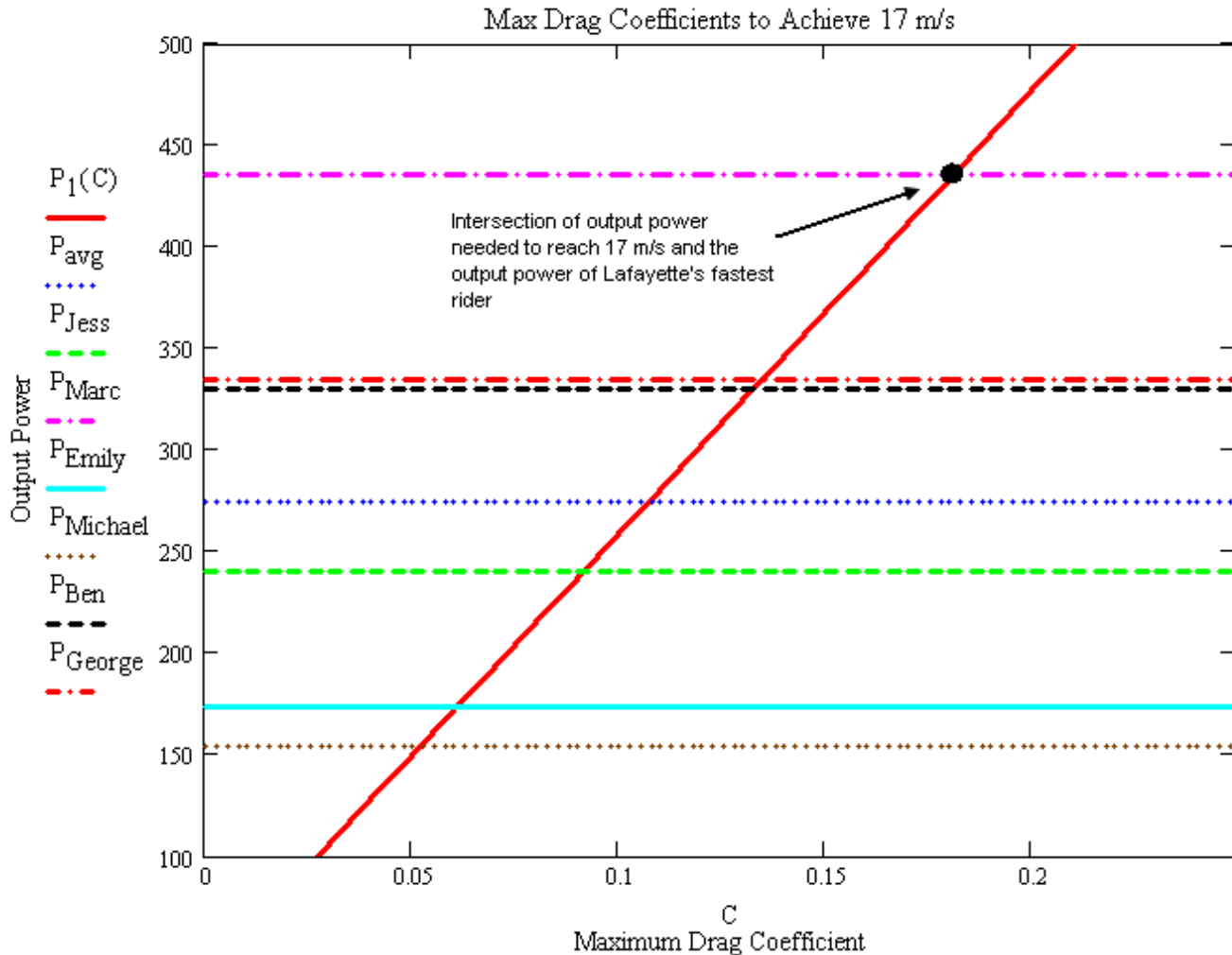
Figure I. 2 Reduction of Experimentally Obtained Data to Calculation Drag Coefficient.

Finally, the team set the feature of HPV adjustability as a key outcome target. Noticing the bimodality of the height distribution of the team members, it was determined that the seat should have a minimum of two settings: one for the taller group of riders and the other for the shorter group. After measuring the relevant extremities of each of the team members, the difference between the two settings was found to be 7 inches. Ultimately, the engineering solution to the problem of adjustability allowed for the easy implementation of more than two seat position settings. The final design permits each rider to operate the vehicle in a position which maximizes her/his power.

3. Selected Review of Supporting Literature

The literature documenting woman and man's endeavors to harness the power of one's own body for transport is quite voluminous. This section attempts to summarize a small representation of that wealth of knowledge as it applies to modern recumbent bicycles and augments the team's findings in its own research (See *Section III, Testing and the Iterative Design Approach*)

Many authors provide means of quantifying the power output of a human. Knowing this datum was an *a priori* task for completing first order models. In the text Human-Powered Vehicles, Abbot and Wilson indicate that an individual on a bicycle should output power on the order of 350 W. They also note that human power output begins to decrease after 20 minutes; hence, the team decided to rotate riders at least every 20 minutes (p. 32). This power output model was later refined with experimental data.

The literature indicates that vehicle dynamics are governed principally by forces imposed on the vehicle from tires, gravity, and aerodynamic drag (Gillespie, p. 5). The general equation for braking performance may be obtained from Newton's Second Law. According to Gillespie, assuming that forces on the vehicle will be constant, simple relationships can be derived. These are presented here as *Equation I.1* (p. 46). This assumption is valid when riding at a constant speed and also while braking at a constant deceleration, i.e., when acceleration and jerk are zero, respectively.

$$\int_{V_0}^{V_f} 1\, dV = \frac{-F_{xt}}{M} \cdot \int_{0}^{t_s} 1\, dt$$

Equation I. 1 Simplified Newton's 2nd Law as a function of time *Fundamentals of Vehicle Dynamics, 1992.*

In this equation, F_{xt} is the braking force, M is the mass of the HPV and rider, V is velocity, and t is time. Since one of the requirements is to stop from a specified velocity (15mph), one can solve for the required braking force. Solving for F_{xt}, Gillespie obtains:

$$F_{xt} := \frac{V_o^2 - V_f^2}{2} \cdot \frac{M}{x}$$

Equation I. 2 Simplified Newton's 2nd Law as a function of distance *ibid..*

As aerodynamic drag is proportional to the square of the speed, it is crucial to minimize drag at high speeds (greater than 20 mph). The targeted sprint velocity is greater than this speed; therefore, minimizing this force is a critical design consideration (Gillespie, p.80).

Several authors provide empirical models for aerodynamic drag and component selection and sizing. Articles by Haake and Martin are discussed in various sections and addenda of this paper.

4. Chosen Engineering Solutions and Discussion of Alternatives

Frame Material

Table I.3 summarizes the relevant design considerations for the frame material as determined from the goal/constraint maps.   Designing the frame with these factors in mind resulted in a structure that is both sufficient for competition needs and uncomplicated.

Table I. 3 Goal/Constraint Map Results for Frame Material Selection.

Examination of the goal/constraint maps indicated that the frame material selection should be dictated by:	
• Strength (robustness) ***	• Cost **
• Manufacturability ***	• Weight *
Where a greater number of asterisks indicated higher importance.	

Traditionally, aluminum, carbon fiber, titanium, and steel are used in bicycle construction. Each material was considered for the frame and is discussed in turn. Carbon fiber, though strong and lightweight, was judged to be prohibitively difficult to work with for construction. Titanium was eliminated due to expense. Aluminum and steel were both considered viable materials for the construction of the frame. The most notable advantage of aluminum is its low weight. However, drawing upon the empirical research conducted by Martin (See *Addendum C, Aerodynamic Calculations*) concerning cycling power, the team concluded that while weight plays a role in the acceleration of a vehicle, it is not a significant criterion for maximizing and maintaining HPV speed on a level surface. Moreover, further investigation into welding techniques indicated that steel is significantly easier to weld than aluminum. Ultimately, the team chose to implement steel for its ease of fabrication. The team made an early decision to use tubular members for their strength and weight characteristics and the ease of obtaining the raw materials from which to fabricate them. Of the many readily available alloy steel tubing, Chromium-molybdenum steel was favored for its strength.

Upright / Recumbent / Prone

Empirically, bicycles have been determined to be one of the most efficient uses of human power for propulsion. It was thus agreed that the HPV design would build upon the design of modern bicycles. Often, incorporating the robust and efficient bicycle components available on the market aids in assembly and reduces the need for costly fabrication.

The team considered three general bicycle configurations determined by the position of the rider: *Upright*, in which the rider sits in the conventional position; *recumbent*, in which the rider sits reclined with feet extending forward; and *prone*, in which the rider lies face down with head pointed in the direction of travel.

Creating a vehicle that rides low to the ground presents greater opportunity for minimizing frontal area and, consequently, reducing drag. Recognizing that the majority of a cyclist's power is utilized to overcome aerodynamic drag (Martin, 2003), the team concluded that keeping the

HPV frame low to the ground was a priority. An upright bicycle design is less desirable as it requires the rider to remain in the most vertical of positions with the greatest amount of body area susceptible to drag forces. Ultimately, a recumbent design was pursued. The recumbent design allows the rider to remain in a comfortable and more natural position than that provided in a prone design—a major consideration in endurance racing.

Number of Wheels / Driving Wheel

A reasonable number of HPV wheels ranges from two (minimum number for line-contact stability) to four (allowing for planar-contact even in conditions where one wheel lifts from the ground-plane). Planar-contact type wheel configurations (three- and two-wheel designs) are more difficult to steer than line-contact designs, as it is more difficult for the rider to capitalize on the dynamic forces created by leaning. Thus, a two-wheel configuration allows for sufficient balance and the ability to decrease the amount of deceleration necessary on turns by banking. Additionally, such a vehicle is narrower (hence more aerodynamic). With the two-wheel design in mind, the team chose the front wheel as the steering wheel and the rear as the drive wheel. This allows for greater responsiveness of the steering, as the lead wheel initiates the change in direction and eliminates the need for a complex coupling of steering and driving capabilities on a single wheel.

Wheelbase

The literature describes two basic recumbent designs. One design features pedals in the front of the leading wheel while the other design has the pedals behind the front wheel. The advantages of the design with the pedals in the front are that the vehicle is lighter because the frame is shorter, the position of the rider can reduce aerodynamic drag, and the shorter wheelbase allows for sharper turns (Abbot and Wilson, p. 118-123).

Staying low to the ground and maintaining comfortable riding positions led to the selection of the smallest available front wheel and fork size. The geometry of the front of the frame was then designed to a) eliminate interference between rider's feet and the front wheel while turning, and b) accommodate the average leg length of the shorter riders while preserving a comfortable riding position for the taller riders.

Fairing Full / Partial

Research indicated that a fully-faired vehicle is generally more aerodynamic than a partially-faired vehicle, as the full fairing allows for greater control of air flow over the object and minimizes pressure drop at the rear of the vehicle. To this end, the team aimed to create a full vehicle fairing which could be easily adjusted to allow quick rider entrance and exit. The team recognized the fact that a solid structure was necessary at the front of the vehicle in order to maintain shape in response to the direct, maximum force of drag. It was thus decided that the HPV would feature a "nose" fashioned from coroplast® (corrugated polypropylene) strips and a transparent polycarbonate windshield. A similarly shaped structure, made entirely of coroplast®, is attached to the rear of the vehicle. Spandex stretches between the two solid structures, creating a fully-covered vehicle with an ellipsoidal shape. The fairing is open-bottomed, allowing the rider to stabilize the vehicle with her/his feet. An easily opened flap was incorporated into the spandex side of the fairing to facilitate quick rider entrance and exit.

B. Innovation and Notable Features

1. Adjustable Seat

The most striking feature of Lafayette College's first entrant into the HPV challenge is the seat, which adjusts position for riders ranging in heights from 5'5" to 6'8". Designing such a wide range of seat positions was important to the team, as it allows for many to enrich their lives with the joy and thrill of HPV riding. Such consciousness of inclusion of different body sizes is a realistic and important attribute in modern design. The design process occurred in three stages, which are pictured from left to right in *Figure I.3*: 1 - angle determination, 2 - adjustability solution, and 3 - weight distribution.
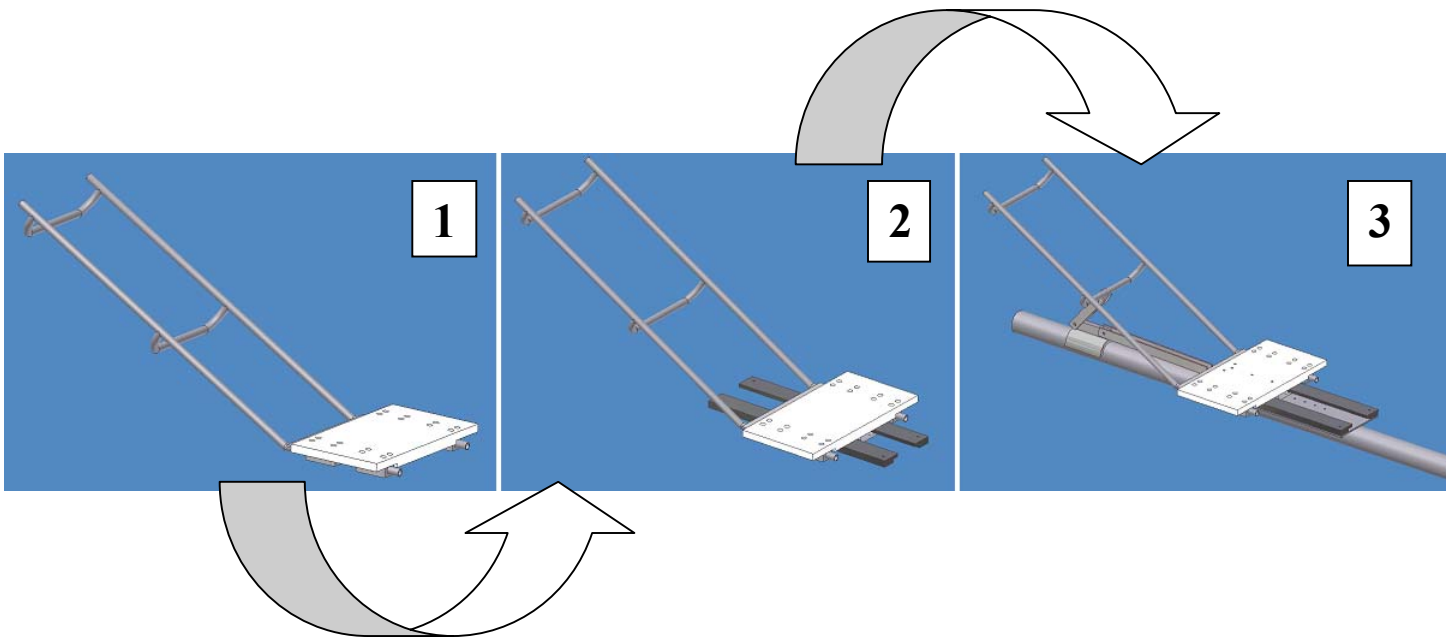

Figure I.3 Three stages of seat design process.

In designing a comfortable and adjustable seat, the team first determined the reclining angle at which each rider felt relaxed and able to produce as much pedaling power as possible. It was discovered that all riders are comfortable with their bodies angled in nearly the same position. A seat frame was modeled to allow riders to maintain this position while pedaling.

The team then devised a simple and effective method for securing the seat to the HPV frame while allowing the seat to slide forward and backward to accommodate the different riders. As illustrated by *Figure I.4*, the updated seat design features a surface on which the rider sits that includes a T-section. This T-section rests on a bottom plate cut from steel and slides along a PVC channel. The bottom plate is welded to the main tube of the HPV frame and gusset plates are attached for added support. Holes are drilled into the steel plate to receive retractable pins inserted in the sitting surface. The seat is thus moved forward and backward along the horizontal tube by lifting the pins, moving the sitting surface to the desired location, and allowing the pins to fall into the appropriate holes in the steel plate.
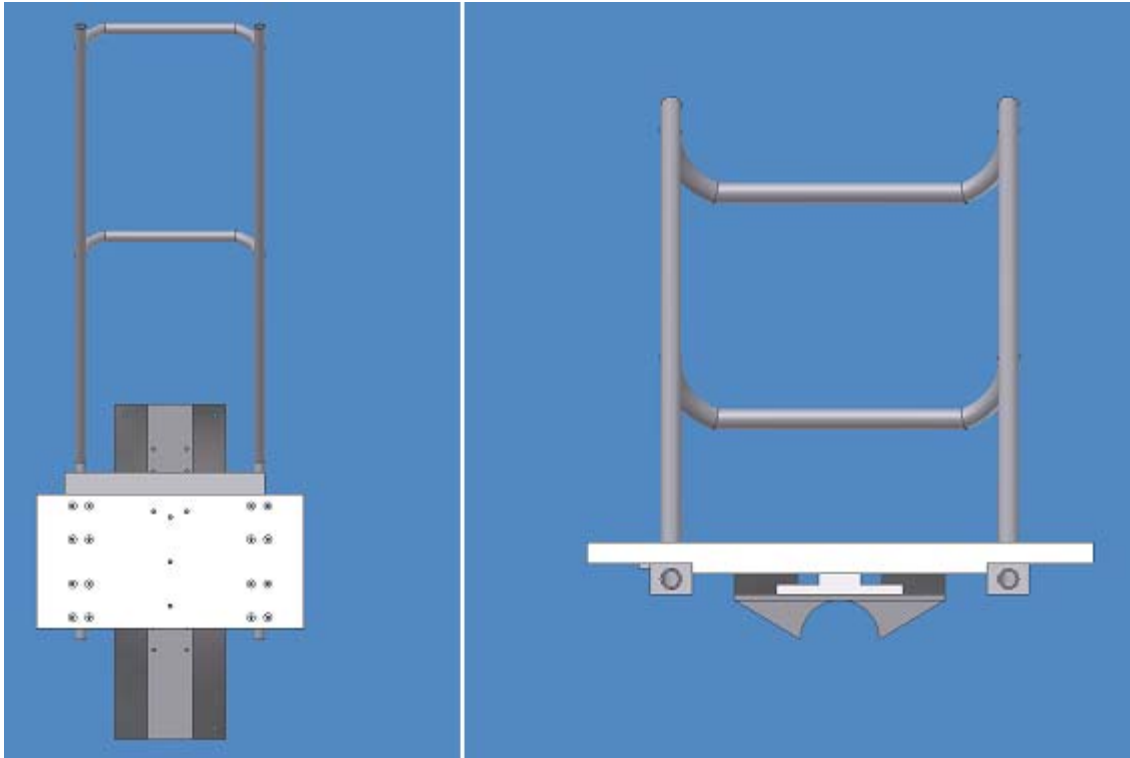
Figure I.4 Top and front view of sliding seat structure.

Ultimately, it was decided that a truss support would be added to the back of the seat. As seen in *Figure I.5*, the truss features lightweight aluminum U-channel members attached to the steel frame of the seat back and an aluminum slider. The slider is lined with a Delrin® brand acetal resin bushing, which rests on the horizontal tube and slides with minimal friction. Rider weight is thus distributed more evenly throughout the seat by way of the truss (refer to *Section III.B, Testing to Develop and Verify Design* for a more fulsome explanation of this weight distribution).
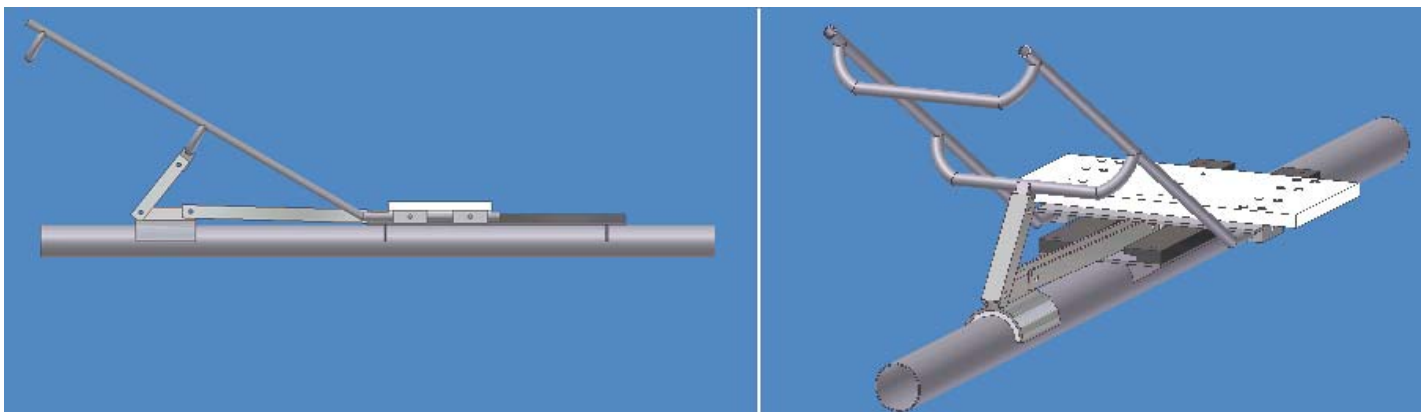

Figure I.5 Side and rear isometric view of seat assembly with truss.

2. Chain Solutions

Housing the crankset in the very front of the recumbent and the cassette in the rear necessitates a very long chain. With a long chain there is more sway or slop, which can present problems when shifting. Additionally, chain slop can cause the chain links to bunch, potentially damaging the chain or derailleur. In extreme cases, chain sway and bunching could cause the chain to disengage from the vehicle, resulting in a safety hazard and disabling the vehicle.

The team found three solutions to this problem. First, the HPV features a mountain bike rear derailleur with a long cage so as to take up as much tension in the chain as possible. Second, an additional tensioner was mounted near the rear of the vehicle to take up the remaining slack. Third, in order to direct the chain so it clears the rider and other moving parts of the HPV, two chain directors are welded to the frame guiding the chain so that it closely follows the contours of the frame. These chain directors are made from re-engineered mountain bike derailleurs. *Figure I.6* illustrates the team's chain solution.
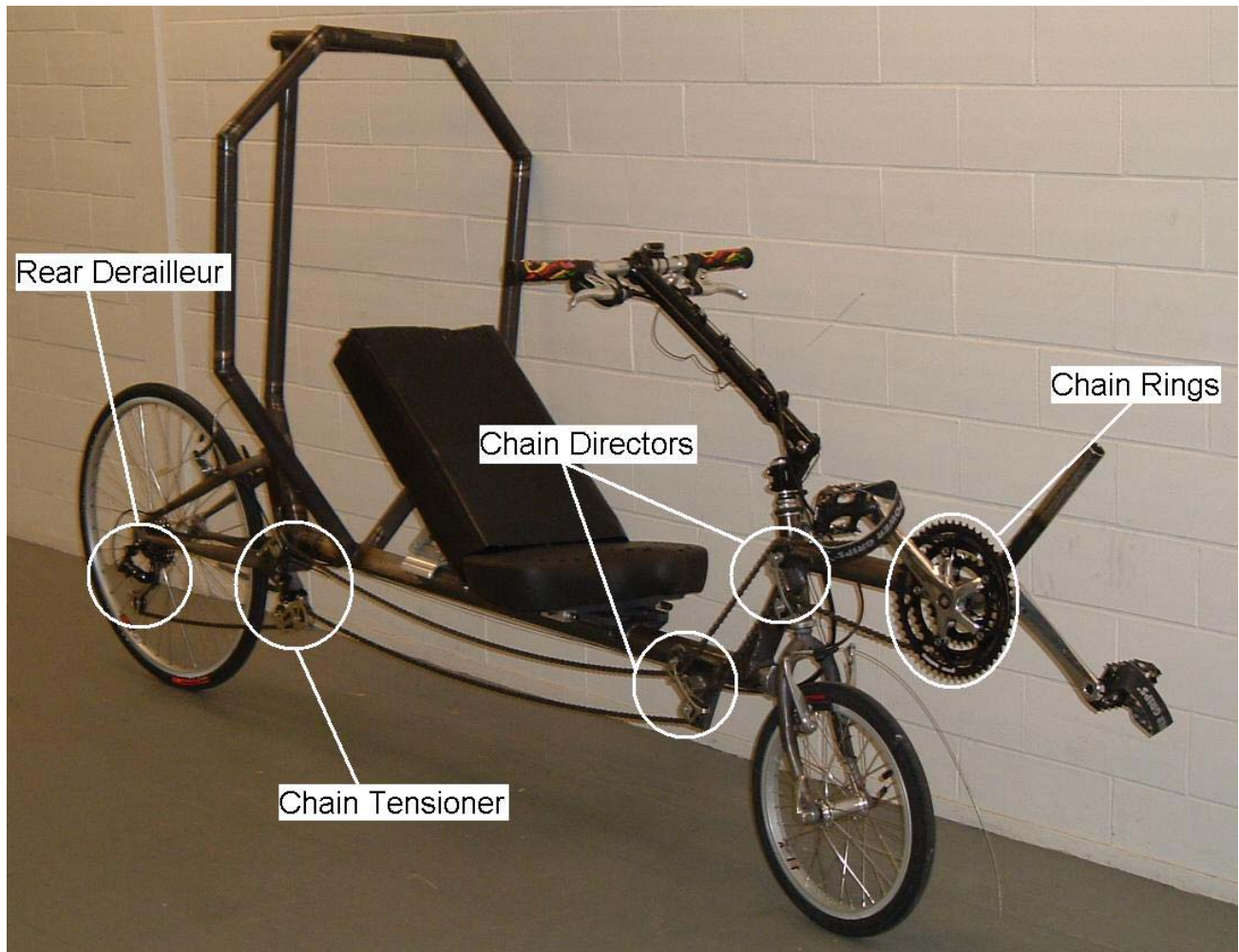

Figure I.6 HPV with components for chain operation.

II. Analysis and the Finite Element Method

Modern parametric modelers offer the engineer a previously unfathomable ability to refine designs before production. Changes in parameter values are updated virtually instantaneously, allowing for immediate determination of material interferences, ergonomic interaction, and aesthetic value. Modern computing also empowers the engineer to solve colossal matrices of simultaneous equations. The Finite Element Method allows for numeric analysis of complex systems. The team employed Finite Element Analysis to safely design the HPV frame.

A. Frame Design and Finite Element Analysis

After the relative position of each frame member was decided by examining ergonomic and mechanical considerations, the exact dimensions of the raw materials used to build the frame needed to be determined. The tubular frame members were parametrically modeled and assembled using AutoDesk Inventor 7©. Finite element analysis results from ANSYS 7.1© were consulted to select the cross-sectional dimensions whenever possible. These analyses are discussed below. The outside diameters and wall thickness of the tubes were then quickly adjusted and the model updated to reflect said changes. In order to facilitate welding, attempts were made to select the same wall thicknesses for any tubes to be welded together; however, some of the desired combinations of sizes were unavailable from the team's suppliers. In such cases, the closest match in wall thicknesses was selected. The thicknesses of all tubes were consequently set as 0.049 inches or 0.058 inches, with exception of the head tube, which required high tolerances to fit the head set (steering bearings). This member was ordered at a thickness of 0.095 inches and reamed to fit the head set specifications.

1. First-order Closed-form Analysis

A simple beam in bending was used as a first order approximation of the horizontal tube, which was assumed to experience the highest deflections and stresses. The loading scheme for the analysis is presented in *Figure II.1*.
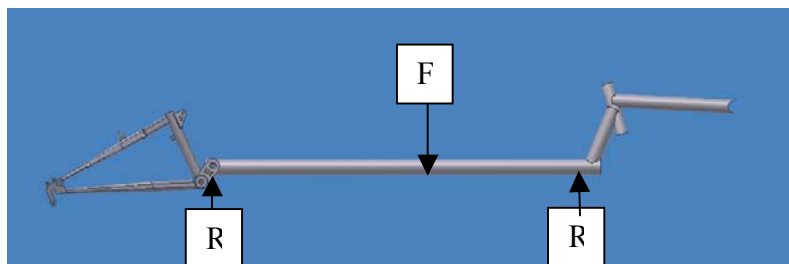

Figure II. 1 Beam-Bending Model.

This preliminary calculation was performed in order to gain a first order understanding of the stresses produced in the HPV frame. This initial analysis indicated that the displacements of the horizontal tube in the vertical direction are four orders of magnitude less than one inch and that the maximum stresses in the tube are an order of magnitude less than the yield strength of 4130 steel. A more robust model was needed to ensure safety, but this model allowed the team to begin the process of design iteration.

2. The Finite Element Model

Confident that the proposed design configuration was reasonably robust, the next step in the analysis of the frame was to build a finite element model and subject it to the multiple forces that it is expected to encounter. The loads associated with a system as complex as an HPV are not only numerous, but less than straightforward to determine. A simplified, basic layout of the frame and its components was modeled and the loads of primary concern (rider's weight and pedaling force) applied. The model boundary conditions and loads are outlined below. A plot of the Von Mises stresses throughout the deformed frame can be seen in *Figure II.2*, while a top view of the deformed frame is shown in *Figure II.3*.
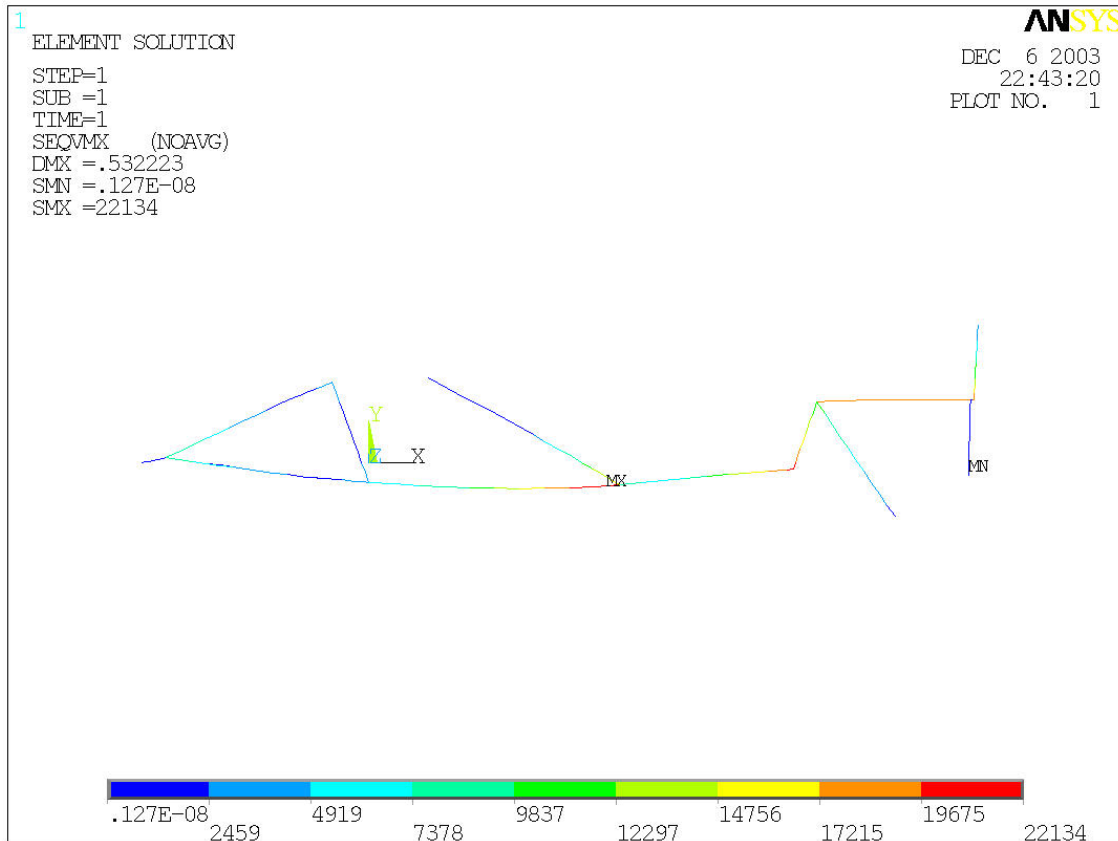

Figure II. 2 Von Mises Stress and Deflection of Frame Model produced with ANSYS 7.1 (c).

The finite element model of the frame includes loads and boundary conditions that, while basic, provided worthwhile results. Boundary conditions and loads were applied at three locations. The frame was constrained at each of the dropout locations—the points at which the frame and the wheels are connected. The rear triangle, which is symmetric about the vertical plane of the HPV, contains two dropouts. One of these points was constrained in all three axial directions in order to fix a point of the frame in space. In contrast, the other rear dropout was fixed in the vertical direction only so as to allow displacement between the two. The third dropout, in the front of the vehicle, was also constrained only in the vertical direction. Under these constraints the wheelbase was free to lengthen and the entire vehicle could displace from the vertical plane.

The loads that caused the frame to displace in these ways include the weight of the rider, the pedaling force exerted on the cranks, and the reaction force on the seat back due to the pedaling force. The weight of the team's heaviest rider (200 lbf) was applied as a point force to the rear of the seat. The pedal force was modeled and applied to be the maximum force in the pedal cycle. This maximum force occurs when the cranks are in their vertical orientation, and as such a pedaling force of 200 pounds was applied to one of the cranks in the horizontal direction (perpendicular to the cranks). The reaction of the pedaling force was applied to the seat back as a point force and is equal in magnitude and opposite in direction to the pedaling force.
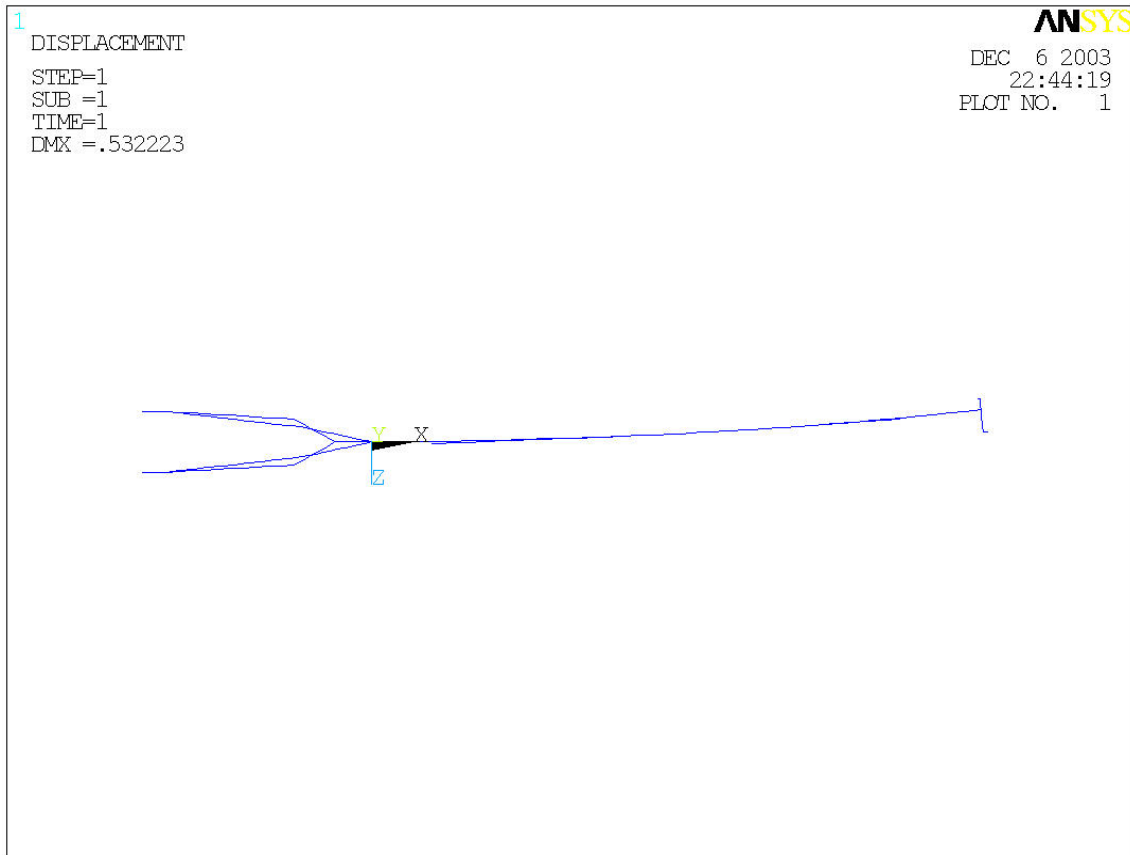

Figure II. 3 Top view of Displacement of Loaded Frame Model produced with ANSYS 7.1 (c).

As indicated in *Figure IV.2*, the maximum stress experienced in the frame is on the same order of magnitude as the yield strength for 4130 steel (~52 kpsi[*]). This result encouraged the selection of the large outer diameter for the horizontal tube, thus increasing the factor of safety. Based on the design limitations associated with utilizing a recycled rear triangle, the maximum allowable horizontal tube outer diameter was found to be 1-$\frac{7}{8}$ in. This analysis suggests that the frame will not experience stresses beyond the yield stress for Chromium-Molybdenum Steel (with a factor of safety of approximately 2.5).

---

[*] Note: this is the yield stress for annealed 4130 steel. This is a rather conservative estimate as it is reasonable that a phase transformation occurred in the welded regions, where the steel may have reached adequate temperatures to return to the γ-phase and was in turn air quenched to form a high strength Martensite.

After more extensive modeling and additional design of the seat were performed the team realized that it was necessary to support the seat in more than one location. A small truss system was designed for this application. Though the truss was designed for integrity of the seat, the change in distribution of the rider's weight to the frame was a serendipitous benefit. *Figures II.4 and II.5* show the changes in stress distribution in the long, horizontal frame member. This loading change not only reduced the critical stress seen in the beam, but also its location. (Note the front of the HPV is at the left-hand side of the figures. The critical stress is now located at the end of the beam, an area which can easily be strengthened by a gusset plate (refer to *II.C, Finite Element Analysis Conclusions and Design Modifications*).
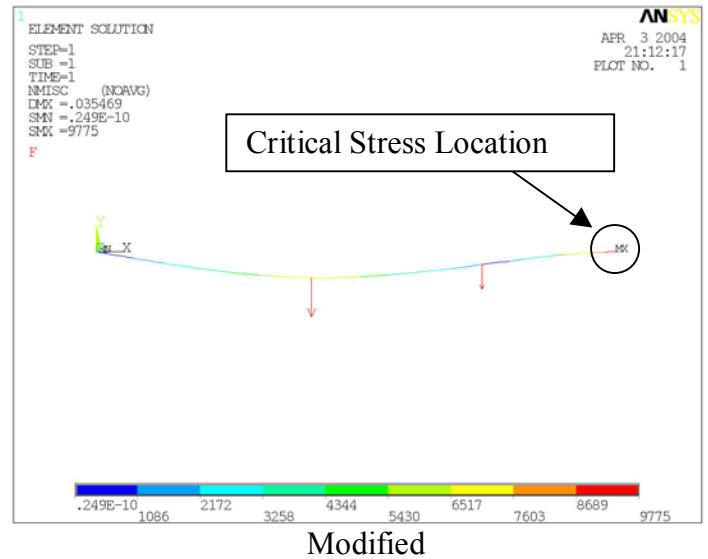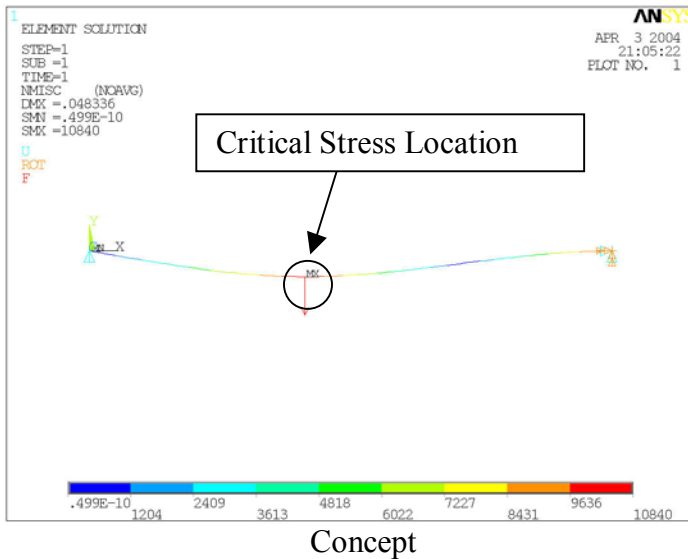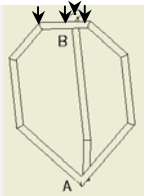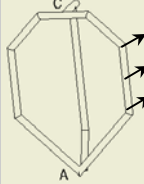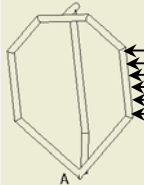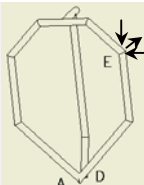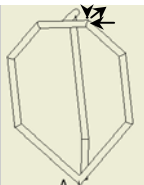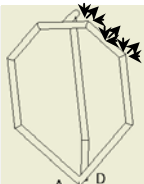

Concept

Modified

Figures II.4 and II.5 Concept and Modified Main Frame Member Model produced with ANSYS 7.1 (c).

B. Roll Over Protection and Finite Element Analysis

The roll cage clearly meets the minimum standard set forth by ASME: it is constructed from 1.5"OD 4130 steel tubing with a thickness of 0.049". However, in order to confirm confidence in the roll cage design, the team created a finite element model, using pipe-style line elements. The team modeled the roll cage attached to the frame, and constrained the frame in six degrees of freedom. Modeling the frame as *terra firma* produces the extreme case of all kinetic crash energy being converted to strain energy entirely within the roll cage members. Seven crash-situations were modeled; the results of which are shown in *Table II.1*. Critically-stressed joints were identified for each case. As previously explained, it is reasonable that the actual strength of the materials in the joints is bounded by the annealed yield strength (52 kpsi) and yield strength for water-quenched 4130 steel (138 kpsi). All critical stress values fall below the annealed yield strength, save for the critical stresses at joint A. The critical value at this location (81 kpsi) is less than the water-quenched yield stress; however, it was determined that an additional strengthening member, a 1/8" steel gusset plate, should be added to ensure the robustness of the roll cage.

Table II.1 Summary of Crash Conditions Modeled with ANSYS 7.1 (c).

	Description of causes of loading conditions	Loading Condition	Critical Locations			Stress Values	
Case One	Simulates an end over end flip. A distributed load of 600 lbf, is applied along the top plane of the roll cage.		**A**	**B**		σ_A=10 kpsi	
						σ_B=8.5 kpsi	
Case Two	Simulates collision with a stationary object. A distributed load of 600 lbf is applied in the direction opposite forward motion.		**A**	**C**		σ_A=20 kpsi	
						σ_C=24 kpsi	
Case Three	Simulates a side impact courtesy of a 2nd vehicle. The distributed load is 600 lbf.		**A**			σ_A=73 kpsi	
Case Four	Simulates tipping while moving. Two forces perpendicular to forward motion result in a diagonal force of 600 lbf. 200 lbf is applied in the direction opposite forward motion.		**A**			σ_A=81 kpsi	
Case Five	Same as case four in a different impact location. This situation would require a partial roll over while moving.		**A**	**D**	**E**	σ_A=25 kpsi	
						σ_D=29 kpsi	
						σ_E=32 kpsi	
Case Six	Same as case four in a different impact location. This situation requires a more extreme roll over than case five.		**A**			σ_A=61 kpsi	
Case Seven	Combines cases five and six with the use of distributed loads. The resultant diagonal force is 775 lbf, while the force in the direction opposite motion is 300 lbf.		**A**	**D**		σ_A=48 kpsi	
						σ_D=38 kpsi	

A   Connection point between the horizontal tube and the diagonal tubes of the roll cage ("V").
B   Connection point between the two top tubes of the roll cage (front, horizontal "T").
C   Connection point between the vertical and horizontal tubes at the rear of the cage ("T").
D   Connection point between the horizontal tube and the diagonal tube at the rear of the cage.
E   Connection point between vertical and diagonal cage tubes, a mitered joint.

C. Finite Element Analysis Conclusions and Design Modifications

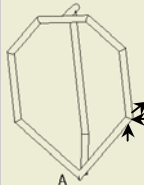The finite element analysis conducted indicated that strengthening members were necessary at three key points on the HPV frame in order to ensure system stability. While the stresses calculated at these points fell below the anticipated yield strengths of the 4130 steel tubing at these points, it was decided that welding gusset plates at these locations would be beneficial, raising the factors of safety to a desirable range. *Figure II.6* shows a model of the HPV with the added gusset plates displayed in red. Plates at Location 1 were added to compensate for the stresses induced by the rider's pedaling action. The gusset at Location 2 strengthens the roll cage and is a direct response to the results of crash-condition 7 as described in *Table II.1*. The plates at Location 3 help to alleviate the stress placed on the horizontal tube due to rider weight.
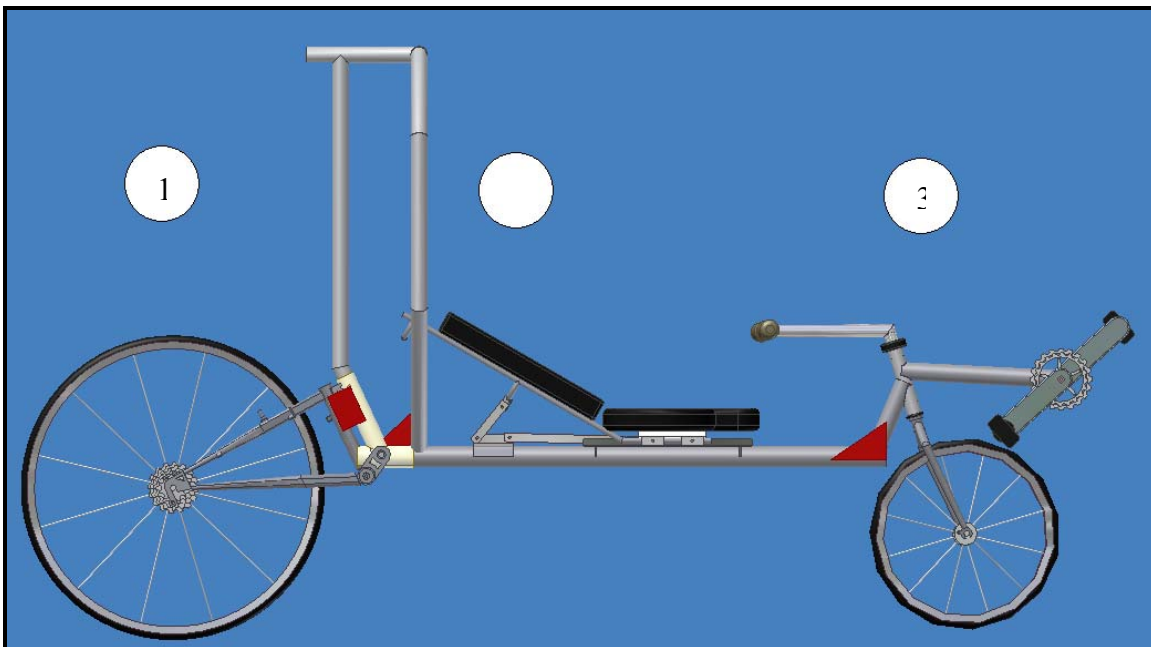
Figures II.6 Gusset Modifications added as a result of ANSYS 7.1 © Analysis.
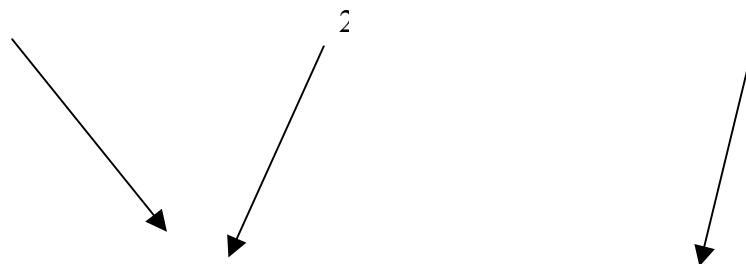
D. Drive Train Analysis

The HPV team decided to implement a drive train with gear-shifting capabilities in order to achieve maximum acceleration and comfort at cruising speeds. The team chose to purchase a rear cassette featuring the smallest possible cog, with 11 teeth, and the largest available front chain ring, with 60 teeth. Utilizing these two components yields the largest gear ratio possible, 5.46, and allows for the slowest pedaling cadence. Keeping this value as the maximum possible gear ratio, the team performed calculations to find the cadence needed to achieve the goal sprint speed (17 m/s) for various wheel sizes.

In researching the pedaling techniques of various bicyclists, the team found that a reasonably fast cadence for the sprint competition is 110 rpm and a reasonable endurance cadence is 70 rpm. The team graphed the cadence necessary to reach 17 m/s at a gear ratio of 5.46 for a range of driving wheel diameters. This plot is presented below as *Figure II.7*. Supporting calculations appear in *Appendix C*. While investigating commonly available wheel sizes, the team observed that the target sprint velocity can be reached with a cadence of 83 rpm when the diameter of the driving wheel is 0.712 meters (28in.)—the standard diameter of a mountain bike wheel including a slick tire. This cadence falls comfortably between the sprint and endurance limits and allows the team to utilize a readily available wheel.
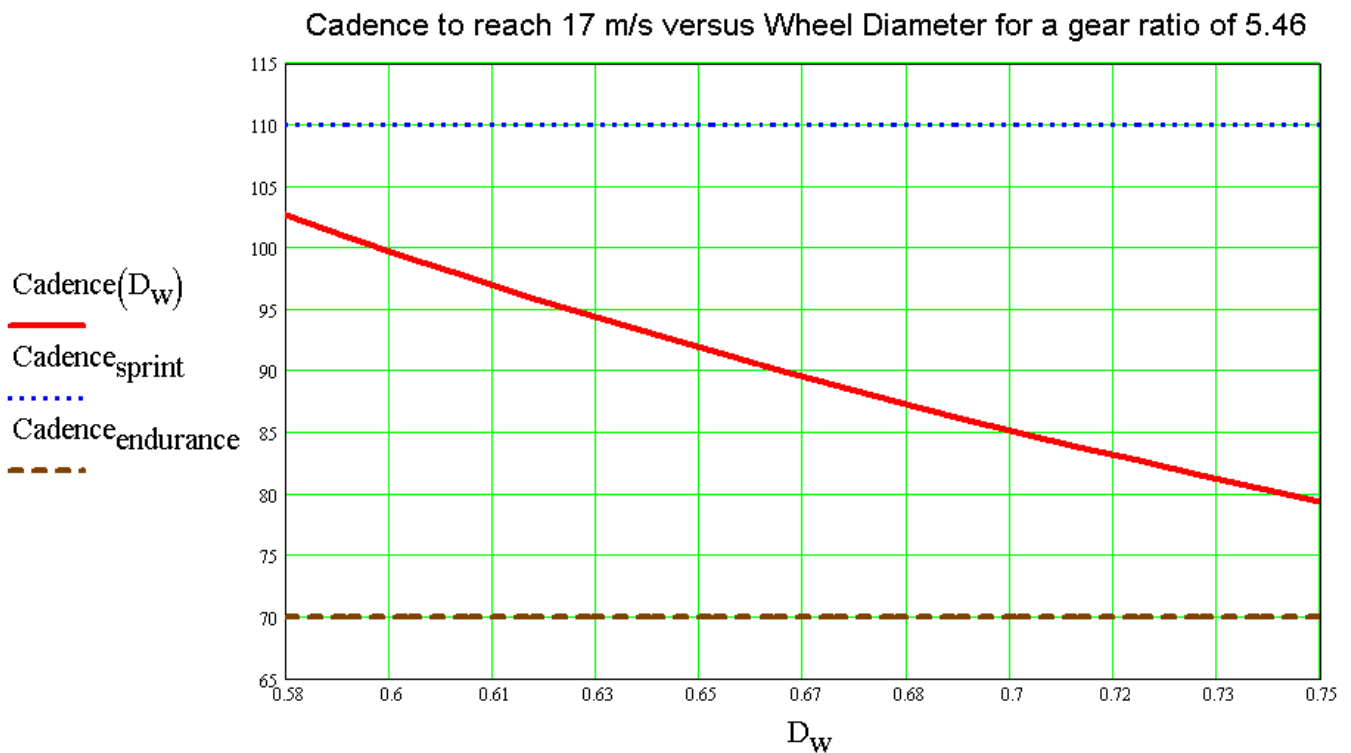

Figure II.7 Plot of cadence necessary to reach goal sprint speed using maximum gear ratio for various driving wheel diameters.

E. Braking Design and Analysis

There are two readily available bicycle braking systems: disk and "V-" style brakes. Disc brakes are heavier and more difficult to set up and keep calibrated than their V-brake counterparts. V-brakes have power that is initially comparable to that of disc brakes, though V-brakes tend to lose some of their power after periods of continued pressure. Such long applications of breaking force should be rare under competition conditions, thus the team decided to implement V-brakes.

Due to their long arms, V-brakes are able to multiply the force applied to the levers by the rider's hand several fold. By measuring the distance from the brake pads to the pivot point and the distance from the cable attachment to the pivot point, the team determined the ratio of output force to input force, i.e., "squeezing force" to braking force to be approximately 1:4 for the Shimano Deore LX V-brakes used on this HPV.

A moderate 20-lb force applied to both (front and back) brake levers would yield 80 lbs of force on each rim surface, i.e., a total of 160 lbf when both brakes are engaged. From *Equation I.2*, shown below, the total braking force required on the wheel rims is 95 lbf. This calculation was performed using 250 lbf as the weight of the vehicle (this is the weight of Lafayette's heaviest rider and the HPV) and applying the ASME guidelines for minimum stopping distance: initial velocity of 15 mph, final velocity of 0 mph and 20 ft for the stopping distance.

$$F_{xt} := \frac{{V_o}^2 - {V_f}^2}{2} \cdot \frac{M}{x}$$

Equation I.2 Stopping force exerted by brake on rim surface, from Gillespie, 1992, repeated for convenience.

In conventional upright bicycle designs the amount of braking force that can be applied to the front wheel is limited by the possibility of flipping the bike. In contrast, a recumbent, with its longer wheelbase and lower center of gravity, has little possibility to flip, thus both brakes can be utilized.

F. Steering Design and Analysis

The HPV steers with the front wheel, employing a conventional stem and handlebar setup. It was decided that controlling the rear wheel would necessitate complicated linkages that would not only be difficult to design and de-bug, but would also be unconventional and unfamiliar to the riders. Similarly, the decision to involve a conventional handlebar was made out of a lack of experience with, and confidence in, Under Seat Systems (USS) that utilize linkages to allow riders to steer with their hands at their sides instead of in front of their chests.

Experimental and analytical methods were employed for determining the range of angles that the front wheel would need to be rotated in order to accomplish the 25-foot turning radius. A simple geometrical analysis of the frame as it applies to the turning radius of the HPV was carried out using AutoCAD. This calculation was performed while assuming a wheelbase of 60 inches and indicates that the two wheels must be offset by 12 degrees from one another in order to achieve the required turn. This result was verified experimentally using a standard upright bicycle with a wheelbase of approximately 45 inches. An arc of radius 25 feet was traced on flat ground and followed while riding the upright bicycle. The angle invoked was ~10 degrees—a reasonable agreement with the analytical results.

III. Testing and the Iterative Design Approach

Various tests allowed the HPV team to glean valuable data for design and to fine-tune performance. While published empirical models and sound engineering principles serve as the basis for development of design models and analysis, test data provides concrete information and guidance in the engineering process. Careful attention to test results and an iterative design approach help prototype models such as this one realize their full potential. Refer to *Addendum D. Drive Train Calculations and Experimental Data* for a summary of testing results.

A. Testing after Fabrication

Performance testing was carried out in an effort to determine the optimum gear ratios for specific aspects of competition performance. The cassette (rear cogs) is a purchased component and offers a fixed range of gears with specific sizes. To simplify the operation and fabrication of the HPV, the team decided to omit the use of a front derailleur. This limitation dictates each rider to choose one front chain ring for the duration of their ride. The chain can be positioned manually to the chain ring chosen by the rider. The team designed tests primarily to verify the design assumption that a front derailleur was not necessary, i.e., no single rider used a range of gearing beyond that available with one chain ring. These tests also determined which of the available chain rings is best suited for each portion of the competition. All tests were performed by each member of the team on a smooth, flat, asphalt surface.

The HPV team acquired chain rings of four different sizes; 60-tooth, 52-tooth, 42-tooth, and 28-tooth. Sample testing indicated that the 28-tooth and 60-tooth chain rings were impractical as they over-limited top speed or acceleration, respectively. Therefore, four tests were performed using the 52- and 42-tooth chain rings: (1) comfortable cadence, (2) straight acceleration, (3) acceleration out of a 90-degree turn, and (4) maximum achievable speed.

1. Cadence

The cadence testing was a comfort test designed to provide information about individual riding preferences and supply target speeds for subsequent tests. The endurance race necessitates that each rider pedal to achieve the fastest speed possible over an extended period of time. The test was thus designed to determine each rider's capabilities. Testing one chain ring at a time, each team member pedaled several laps around the testing track to determine what maximum speed she/he would be comfortable maintaining during the endurance race. The rider noted which rear gear was used to achieve this comfortable cruising speed. This information was later used to calculate cadences [rpm].

The results of this test indicate, unsurprisingly, that using either of the two tested chain rings for the endurance race will be feasible for all of the riders. With the 52-tooth ring every member of the team used either the 20- or 23-tooth rear cog, with comfortable speeds produced ranging from 14 to 18.25 mph. This data indicates that when using the 52-tooth ring the team finds cadences between 74 and 84 rpm to be comfortable. Results from tests done with the 42-tooth chain ring are similar, but show more variance. The range of comfortable speeds is the same as in the 52-tooth test, but the rear cogs used to achieve these speeds varied from 11 to 20 teeth. The combinations of speeds and rear gear sizes resulted in cadences ranging from 58 to 83 rpm.

The cadence testing compares favorably to the values used in *Section II.D, Drive Train Analysis*. In these calculations a nominal published cadence value of 70 rpm was used as the lower limit in the calculation to select wheel size. Average values from the testing confirm that this assumption is reasonable.

2. Straight Acceleration

The straight acceleration test was completed with the use of a timer and calibrated digital speedometer attached to the HPV. The goal of this exercise was to determine which of the available chain rings best facilitates rapid acceleration for the endurance race. In this test, both rings were tested for acceleration from 10 mph to 15, 20, and 25 mph. In performing the test, the chain was run over a designated chain ring and the rider used whichever rear gear she/he felt was most comfortable to propel the vehicle at a constant speed of 10 mph. Upon signaling to the timer, the rider began to accelerate as fast as possible to a final speed of 25 mph. While accelerating, the rider changed rear gears as she/he saw fit and indicated to the timer when each increment of 5 mph had been achieved. Note that some of the higher speeds proved unattainable for some riders in the limited space available for testing.

The results of this test, presented in *Table III.1*, proved to be particularly useful in that they indicate unequivocally that the smaller of the two tested chain rings is better suited for acceleration over a range of 10 to 25 mph. Accumulating all of the recorded data and calculating team averages for accelerations between each speed increment and over the 10-25 mph range shows that the 42-tooth ring has a greater acceleration than the 52-tooth ring in every category. The accelerations for the 42- and 52-tooth rings over the 10-25 mph range are 1.21 mph/s (0.54m/s^2) and 0.92 mph/s (0.41m/s^2), respectively.

Table III.1 Straight Acceleration Data.

Rider	52 - tooth Time to 15 [sec]	Gearing Avg Acceleration [mph/s]	Time to 20 [sec]	Avg Acceleration [mph/s]	Time to 25 [sec]	Avg Acceleration [mph/s]
Ben	2.50	2.00	6.00	1.43	11.50	0.91
Marc	4.50	1.11	11.50	0.71	19.25	0.65
Jess	4.00	1.25	9.00	1.00	19.00	0.50
George	4.50	1.11	10.75	0.80	17.50	0.74
Michael	6.50	0.77	12.00	0.91	*	*
Emily	5.70	0.88	19.60	0.36	*	*
Avg.	4.62	1.19	11.48	0.87	16.81	0.70
	42-tooth Time to 15 [sec]	**Gearing** Avg Acceleration [mph/s]	Time to 20 [sec]	Avg Acceleration [mph/s]	Time to 25 [sec]	Avg Acceleration [mph/s]
Ben	2.50	2.00	5.60	1.61	9.00	1.47
Marc	5.00	1.00	9.50	1.11	14.50	1.00
Jess	5.00	1.00	9.00	1.25	14.00	1.00
George	2.00	2.50	5.75	1.33	9.75	1.25
Michael	4.50	1.11	12.00	0.67	18.00	0.83
Emily	4.20	1.19	19.00	0.34	*	*
Avg	3.87	1.47	10.14	1.05	13.05	1.11
*did not attain speed in given course						

3. Acceleration out of 90-degree turn

The test for acceleration out of a 90-degree turn was performed with the dual purpose of verifying the results of the straight acceleration test and practicing the execution of the sharpest turn featured in the endurance competition. This test again required the use of the speedometer and timer. A 25-foot radius was marked using cones and a line of tape. Each rider maneuvered through the turn at the fastest speed with which she/he was comfortable. Note that these speeds were slower than the comfortable cruising speeds determined earlier for each rider. Upon exiting the corner, the rider took note of her/his speed while the timer was triggered. The rider then accelerated to the comfortable cruising speed and indicated when this speed had been reached. The time elapsed between exiting the corner and reaching the comfortable cruising speed was recorded for each rider using each of the chain rings.

The results of the previous acceleration test were supported by the outcome of this exercise as the average team accelerations for the 42- and 52- tooth chain rings were 0.67 mph/s (0.3 m/s^2) and 0.58 mph/s (0.26m/s^2), respectively. Additionally, the test was valuable in that it accurately simulated endurance race conditions.

4. Maximum Speed

A fourth test was conducted to determine whether or not the 52-tooth chain ring (and possibly the 60-tooth ring, with the fairing attached to the vehicle) will be useful in the sprint competition. Each rider propelled the HPV as fast as possible using both the 42- and 52-tooth rings. It was found that while some riders were able to achieve top speeds with the 42-tooth ring that were equal to, if not greater than, the top speeds that they were capable of reaching with the 52-tooth ring, the team's more powerful riders were able to achieve a fast enough cadence with the 52-tooth ring to noticeably surpass the highest speed that they reached using the 42-tooth ring. This indicated to the team that the 52-tooth chain ring would need to be used in the sprint competition in order to achieve the maximum possible speed.

B. Testing to Develop and Verify Design

1. Development:

Early in the design process, the team used recumbent exercise bicycles to gather experimental data for each rider's cycling ability. Recording the number of kilocalories burned and the time elapsed while cycling over a distance of three miles, the team was able to calculate individual power outputs. These data were utilized to calculate the maximum HPV drag coefficient that allowed the team's fastest rider to reach the target sprint velocity of 17 m/s. This coefficient was found to be 0.18. Drawing upon White's research, the team decided to design an aerodynamic fairing having a shape ellipsoidal in nature with a major to minor axis ratio of 4. This shape yields a drag coefficient of roughly 0.1 (White, p. 485).

2. Verification:

As an original fabricated assembly, the HPV seat required testing of its structural integrity. Upon consulting machinists and welding technicians regarding material selection for making the frame, it was decided that 4130 Chromium-Molybdenum steel tubing of 0.058" thickness would be utilized for its malleability and ease of welding. Upon examining the angle at which the rider would be positioned in the HPV, the team observed that the back of the seat frame would support a great amount of the rider's weight and the dynamic reaction force from pedaling. This prompted the team to design a truss system that would reinforce the back of the seat frame while still enabling the seat to adjust to various positions. Preliminary calculations were made to determine a reasonable geometry for the truss configuration using readily available materials. Engineering drawings were produced using these calculated geometries and seat components machined. With the seat construction complete, the truss and seat design operated flawlessly. In order to verify the necessity and integrity of the truss system, two simple tests were performed. These tests determined the magnitude of the force that the truss system would be supporting.

The tests were designed to simulate the forces acting upon the seat while the rider is at rest and while she/he is pedaling. Two O'Haus scales were positioned beside one another and at different heights in order to reproduce the angle at which the seat assembly rests on the horizontal tube. The seat was removed from the HPV and positioned on top of the scales as shown in *Figure III.3*. Scale 1 recorded the vertical force that the horizontal portion of the seat would experience, while Scale 2 recorded the vertical force that the angled back of the seat would face. The scales were zeroed with the seat in placed. The team's two heaviest riders were employed to simulate the maximum forces that the seat would undergo. Each rider sat on the seat with legs resting against a wall (the wall representing the HPV pedals). The measured weights were recorded; thus, the test determined the forces on the seat under static conditions. Next, each rider positioned her/himself with feet against the wall, this time pushing off the wall to simulate the action of pedaling. This test determined the reaction forces for the condition of pedaling.

Figure III.1 Schematic of Seat Testing.
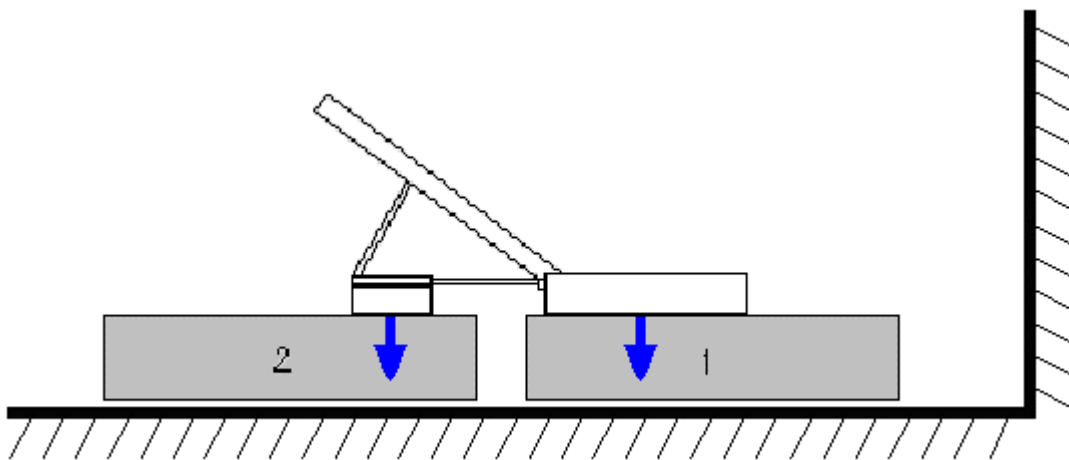
It should be noted that the sum of the scale readings for each rider was always less than the rider's weight. While this result initially seemed counterintuitive, it is feasible since the rider's weight was partially supported by the vertical frictional force between his feet and the wall. It seems feasible that this phenomenon actually occurs in the HPV as well, since the vehicle pedals

support a portion of the rider's legs. The force distribution was approximately the same for both riders in each test. In the static test, approximately 60% of the vertical force was exerted on the seat base, whereas the dynamic test yielded approximately 40% of the vertical force being exerted on the seat base. These results are summarized in *Table III.2*.

Table III.2 Weight distribution test results

Rider	Rider's Total Weight (lb)	Resting feet on wall			Pushing against wall		
		Scale 1 (lbf)	Scale 2 (lbf)	Sum (lbf)	Scale 1 (lbf)	Scale 2 (lbf)	Sum (lbf)
Ben	200	115	75	190	70	110	180
Marc	190	105	68	173	75	98	173

For the heaviest rider, the dynamic force on the back of the seat was a rather high 110 lbs. Using this value as the maximum force in the vertical direction, a bending stress calculation was performed on the back of the seat frame (without inclusion of the truss system) using ANSYS®. One side of the frame was modeled and constrained and half of the maximum vertical force was applied. A maximum Von Mises stress of 97 kpsi occurred at the bend in the frame (*Figure III.2*). Considering that the material was bent using heat, the steel was considered as annealed. The yield strength of 4130 annealed steel is reported as 52 kpsi. Under pedaling conditions, the stress in the frame is nearly double this value, proving that the truss system is necessary. Analysis accounting for the truss indicates that the final seat design is reasonable robust.
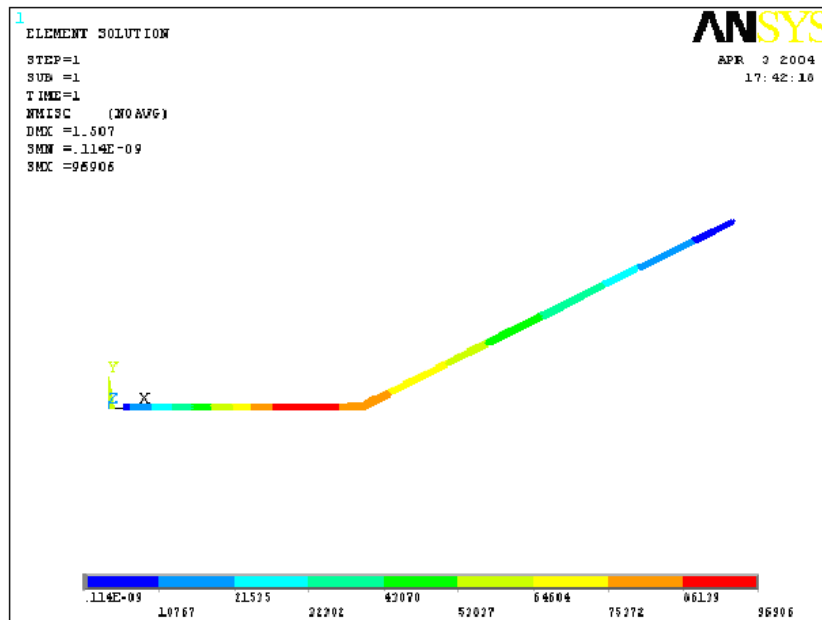

Figure III.2 ANSYS analysis of Weight Distribution on Seat.

IV. Safety and Hazard Reduction

Regulations regarding the health and safety of workers have increased exponentially in the U.S. and abroad in recent years. Due to the rightful recognition of the importance of safety and the litigiousness of society, incorporation of safety analysis is paramount. The team recognized and emphasized the importance safety from the initiation of the project. A goal/constraint map such as the one displayed in *Figure I.1* for the goal of "safe" was one of the first such maps the team completed. Careful consideration of the design elements which control safety led to design and analysis in three areas: materials, seat belt, and rollover protection.

A. Material for Shell

The aerodynamic shell covering the HPV is constructed of safe, lightweight materials. The solid "nose" features clear polycarbonate and coroplast® brand polypropylene. Coroplast® is an especially rider-friendly material, as it is generally soft and pliable. In the event of a crash, the coroplast® will deform slightly, rather than shattering or splintering like other typical fairing materials, such as fiberglass. While the reinforced coroplast® nose and polycarbonate windshield are harder than the other coroplast® strips, they are housed far from the rider's torso and head. Thus, injury to the rider is minimized in the event of a crash sufficient to crack the hard nose cone. Clearly, the spandex stretching over the middle section of the HPV poses no threat to the rider and enables her/him to react without inhibition in response to a crash.

B. Material for Frame

The vehicle frame is constructed of 4130 Chromium-Molybdenum steel tubing with varying outer diameters and wall thicknesses ranging from 0.049" to 0.058". The widespread implementation of 4130 steel tubing in frames for vehicles such as dragsters and go-carts serves as testament to its proven strength and reliability. Typical service and crash conditions for these applications are harsher than those conditions for an HPV; thusly, the tubing is sufficiently strong for HPV applications. Careful welding of the fish-mouthed frame members ensures that the integrity of the steel alloy remains intact. The addition of steel gusset plates at key stress points in the frame solidifies the suitability of the selected frame material (See *Section II.C, Finite Element Analysis Conclusions and Design Modifications* for an explanation of the analysis leading to the development of the gusset plates).

C. Seat Belt

The HPV seat belt restrains the rider across the waist and shoulder, while allowing quick and easy entry/exit. The seat belt is attached to the robust roll cage. This attachment ensures that force applied to the seat belt is grounded to the frame through the roll cage. The team selected a non-retractable, three point seat belt commonly used in go-cart racing. The waist belt, attached to the bottom of the roll cage, prevents the rider from sliding forward in the event of rapid deceleration. The shoulder strap, stretching from the top of one side of the roll cage to the base of the cage, prevents the rider from falling out of the side of the vehicle in a crash situation. Moreover the shoulder strap reduces the distance the body will travel do to inertial forces in a crash situation. Such a reduction in distance reduces the speed and acceleration attained before the body stops and thus the impulse force is reduced upon quick the braking of a crash situation.

D. Roll Over and Side Protection

The roll cage (shown in *Figure IV.1*) protects the vehicle during rolls or flips induced by moments about the x- and y- axes of a standard right-handed coordinate system. This is to say, the HPV can withstand an end-over-end flip or a sideward role. The roll cage is fabricated from 1.5" OD 0.049" thick 4130 Chromium-Molybdenum steel tubing, as per ASME guidelines. The roll cage extends above the tallest rider's head while she/he is seated in the vehicle and serves as the seat belt's ground to the frame, ensuring the rider is securely protected and constrained during crash events. Moreover, as discussed in *Section II.B Roll Over Protection and Finite Element Analysis*, the roll cage is reasonably robust for seven extreme crash situations.

Figure IV.1 HPV with fairing removed to show roll cage.

E. Rider's Field of View

A thin polycarbonate windshield allows for a large, unobstructed field of view. The projected rectangle of vision is approximately 2 ft^2 in area. This area results in 100 degrees of vision, an adequate and safe view of the track during 25-ft radius turns. The windshield also protects the rider's eyes from debris as she/he rides.

Addenda

A. Acknowledgements

The ASME HPV Challenge synthesized all four components of the *Lafayette Experience*: student-focused teaching and mentoring; challenging, broad-based curriculum; small college environment with large college resources; and a friendly community. This unique experience did not happen by accident, but rather it was the union of efforts of many individuals. Of these many professors, mentors, and friends, we would be remiss not to extend special thanks to five:

Harry Folk, Laboratory Technician, Acopian Engineering Center

Richard Merz, Associate Professor of Mechanical Engineering

Richard Reeman, Laboratory Supervisor, Acopian Engineering Center

M. Erol Ulucakli, Associate Professor of Mechanical Engineering

Leonard Van Gulick, Mathew Baird Professor of Mechanical Engineering

Dedicated, generous partners in industry also contributed to this project in meaningful ways. Our gratitude certainly extends to:

Half Scale Dragsters; Phillipsburg, NJ

Genesis Bicycles; Easton, Pa

Broken Spoke; Easton, Pa

Richard Gallagher; Fogelsville, Pa

B. Selected Bibliography

Abbott, Allan V. and David Gordon Wilson. Human-Powered Vehicles. Champaign IL: Human Kinetics Publishers, 1995.

Gillespie, T. D. Fundamentals of Vehicle Dynamics. Warrendale, PA: Society of Automotive Engineers, 1992.

Haake, Steve. The Engineering of Sport. Brookfield, VT: A.A. Balkema; Rotterdam, 1996.

Martin, Jim. Aerodynamics of Cycling. Last assessed November 30, 2003. <http://www.cervelo.com/tech/articles/article5.html.

"Threaded-type Headset Removal, Installation and Adjustment." Park Tool, Co., © 2003. <http://www.parktool.com/repair_help/howfix_headset.shtml>

White, Frank M. Fluid Mechanics. Fifth ed. New York: McGraw-Hill, 2003.

Addendum C: Aerodynamic Calculations

Determination of Drag Coefficients:

Variable Assignments:

C: Coefficient of Drag

P: Power Input (W)

A: Frontal Area of Vehicle (m^2)

V_g: Ground Velocity (m/s)

F_w: Force to Rotate Wheels (N)

V_h: Head Wind Velocity (m/s)

V_a: Net Air Speed (m/s)

μ_{rr}: Coefficient of Rolling Resistance

ρ: Density of Air (kg/m^3)

W_T: Average Weight of Rider and Bike (N)

Assumed Values:

$A_f := 0.73m^2$ Estimation of HPV Frontal area with Fairing

$V_g := 17\dfrac{m}{s}$ Maximum Velocity Goal

$V_h := 0\dfrac{m}{s}$ Assume there is no wind

$V_a := V_g + V_h$

$\rho := 1.184\dfrac{kg}{m^3}$

$\mu_{rr} := 0.00244$

$W_T := 220lbf$ $W_T = 978.609N$

Analysis:

Define Power as a function of C. Note this equation is derived by Martin, 2003.

$$Power(C) := \frac{1}{2} \cdot C \cdot \rho \cdot A_f V_a^{\ 2} \cdot V_a \cdot V_g + \mu_{rr} \cdot W_T \cdot V_g + F_w \cdot V_g^{\ 3} + W_T \cdot V_g \cdot \sin(\operatorname{atan}(RoadGrade))$$

Eq. 1 - Cycling Power (Martin, 2003)

Assumptions:

Neglect power to rotate wheels because it is less than 1%. Assume bike will ride on flat surface, therefore ignore term for power to overcome an incline.

$$P_1(C) := \frac{1}{2} \cdot C \cdot \rho \cdot A_f V_a^{\ 2} \cdot V_g + \mu_{rr} \cdot W_T \cdot V_g$$

Eq. 2 - Simplified Power Equation

Define the weight of the rider + vehicle. The weights of all team members are listed in the range variable below.
The weight of the HPV is estimated as 30 lbs.

Estimated weight of the HPV:

$Wt_{hpv} := 30lbf$

Weight of rider + vehicle:

$Wt := \begin{pmatrix} 135 \\ 180 \\ 165 \\ 135 \\ 200 \\ 185 \end{pmatrix} \cdot lbf + Wt_{hpv}$

The Empirical Power Output data collected using the stationary excercise bicycles was manipulated in earlier calculations to determine the cycling power of each team member. This data is listed as the power range variable (P) shown below.

$P := \begin{pmatrix} 240 \\ 436 \\ 154 \\ 174 \\ 330 \\ 335 \end{pmatrix} W$

$P_{Jess} := P_0$ $P_{Michael} := P_2$ $P_{Ben} := P_4$

$P_{Marc} := P_1$ $P_{Emily} := P_3$ $P_{George} := P_5$

The average team member power output is therefore: $P_{avg} := 275W$

Substituting the average drag coefficient into Equation 2, we obtain an expression for the average power (Eq. 2).

$$P_{avg} = \frac{1}{2} \cdot C_{avg} \cdot \rho \cdot A_f V_a^{\ 2} \cdot V_g + \mu_{rr} \cdot W_T \cdot V_g$$

Eq. 2' - Simplified Power Equation

Rearranging Eq. 2', we obtain an expression for the average coefficient of drag (Eq. 3).

$$C_{avg} := -2 \cdot \frac{-P_{avg} + \mu_{rr} \cdot W_T \cdot V_g}{\rho \cdot A_f V_a^{\ 2} \cdot V_g}$$

Eq. 3 - Average coefficient of friction

Similarly, the coefficient of drag for each individual is defined by Eq. 4.

$$C_{individual} := -2 \cdot \frac{-P + \mu_{rr} \cdot Wt \cdot V_g}{\rho \cdot A_f V_a^{\ 2} \cdot V_g}$$

Eq. 4 - Coefficient of drag for each rider, where $C_{individual}$ is a range variable.

Substituting in values yields: $C_{avg} = 0.107$

$$C_{individual} = \begin{pmatrix} 0.096 \\ 0.182 \\ 0.054 \\ 0.066 \\ 0.132 \\ 0.135 \end{pmatrix}$$

*Note: These are the coefficients necessary to reach our goal velocity of 17 m/s.

Addendum D: Drive Train Calculations and Experimental Data

Drive Train Calculations - Produced using MathCAD

Variable Assignments:

Cadence - rpm of the cranks

C_w - circumference of the rear wheel

D_w - diameter of the rear wheel

V - goal sprint velocity

N_{ch} - number of teeth on the chain wheel

N_{ca} - number of teeth on the cassette

G_R - gear ratio

Analysis:

Determining greatest gear ratio:

$N_{ch} := 60$

$N_{ca} := 11$

$G_R := \dfrac{N_{ch}}{N_{ca}}$ $G_R = 5.455$

Converting sprint velocity to $\dfrac{m}{min}$:

$17 \dfrac{m}{s} = 1.02 \times 10^3 \dfrac{m}{min}$ $V := 1020 \dfrac{m}{min}$

Calculating Cadence as a function of Driving Wheel Diameter:

$D_w := 0.4, 0.41 .. 0.78$ --->   Diameter values will range from 0.4 to 0.78 m

$C_w(D_w) := \pi \cdot D_w$

$Cadence_{sprint} := 110$

$Cadence_{endurance} := 70$ --->   Limits obtained through research

$Cadence(D_w) := \dfrac{V}{G_R \cdot C_w(D_w)}$ --->   Function is plotted

Acceleration out of a 90 degree turn of 25 ft radius

52-tooth	Gearing			
	Exit Speed	Comfort Speed	Time	Avg Acceleration
	[mph]	[mph]	[sec]	[mph/s]
Ben	16.50	19.00	2.60	0.96
Marc	16.50	18.50	4.00	0.50
Jess	15.50	17.00	4.00	0.38
George	16.00	19.00	3.00	1.00
Michael	13.00	14.00	4.00	0.25
Emily	13.00	14.50	4.00	0.38
Average	15.08	17.00	3.60	0.58

42-tooth	Gearing			
	Exit Speed	Comfort Speed	Time	Avg Acceleration
	[mph]	[mph]	[sec]	[mph/s]
Ben	15.50	18.50	3.50	0.86
Marc	17.50	18.50	1.50	0.67
Jess	15.00	17.00	3.00	0.67
George	15.00	18.00	3.25	0.92
Michael	12.50	14.00	3.50	0.43
Emily	13.00	14.50	3.00	0.50
Average	14.75	16.75	2.96	0.67

Average Speed at a Comfortable Cadence for Endurance Race

52-tooth	Gearing			
	Avg Speed	Rear Cog Size	Gear Ratio	Avg Cadence
	[mph]	[teeth]		[rev/min]
Ben	17	20	2.60	78.40
Marc	18.25	20	2.60	84.17
Jess	17	20	2.60	78.40
George	16	20	2.60	73.79
Michael	14	23	2.26	74.25
Emily	14.5	23	2.26	76.91
Average	16.13	21.00	2.49	77.66

42-tooth	Gearing			
	Avg Speed	Rear Cog Size	Gear Ratio	Avg Cadence
	[mph]	[teeth]		[rev/min]
Ben	18.5	13	3.23	68.66
Marc	18.5	13	3.23	68.66
Jess	17	15	2.80	72.80
George	18.5	11	3.82	58.10
Michael	14	20	2.10	79.94
Emily	14.5	20	2.10	82.80
Average	16.83	15.33	2.88	71.83